Sedimentation processes and sedimentary characteristics of tidal bores along the north bank of the Qiantang Estuary

FAN DaiDu[1,2*], CAI GuoFu[1], SHANG Shuai[1], WU YiJing[1], ZHANG YanWei[1] & GAO Lei[3]

[1] *State Key Laboratory of Marine Geology, Tongji University, Shanghai 200092, China;*
[2] *Key Laboratory of Marine Sedimentology & Environmental Geology, State Oceanic Administration, Qingdao 266061, China;*
[3] *State Key Laboratory of Estuarine and Coastal Research, East China Normal University, Shanghai 200062, China*

A tidal bore is a unique Earth surface process, characterized by its highly destructive energy, predictable periodicities and magnitudes, and the production of characteristic sedimentary features. Tidal bores and associated rapid flood flows are highly turbulent flows of the upper-flow regime with a velocity over several meters per second. Reynolds (R_e) and Froude (F_r) numbers, respectively, are larger than 10^4 and 1.0, making them significantly different from regular tidal flows but analogous to turbidity currents. Until now, understanding of tidal-bore depositional processes and products has been limited because of the difficulty and hazards involved with gauging tidal bores directly. The Qiantang bore is known as the largest breaking bore in the world. Field surveys were carried out in May 2010, along the north bank of the Qiantang Estuary to observe the occurrence of peak bores, including regular observations of current, water level and turbidity at the main channel. Several short cores were sampled on the intertidal flats to study the characteristic sedimentary features of tidal bores. Hydrodynamic and sedimentological studies show that the processes of sediment resuspension, transport and deposition are controlled primarily by the tidal bores, and the subsequent abruptly accelerated and decelerated flood flows, which only account for one tenth of each semidiurnal tidal cycle in the estuary. Tidal-bore deposits are generally poorly sorted because of rapid sedimentation after highly mixed suspension by intense turbulence. This behavior is characteristic of the absence of tractive-current depositional components in a *C-M* diagram. It also goes along with well-developed massive bedding, graded bedding, basal erosion structures, convolute bedding and dewatering structures. Together, these sedimentary features can constitute fingerprinting of turbidites, widely distributed in the deep-water environment. However, a tidal bore is triggered by intensely deformed tidal waves propagating into a shallow-water environment, which returns to regular tidal flows rapidly after the passage of the bore head. The tidal-bore deposits are usually bounded by the intertidal-flat deposits with typical tidal beddings at the top and on both flanks. The difference between tidal-bore deposits (TBD) and tidal sandy/muddy deposits (TSD/TMD) is evident not only in sedimentary structures, but also in the grain-size composition. They can be clearly distinguished in grain-size bivariate plots, typically the plot of mean grain size vs. standard deviation (or sorting). Some trend variations generally exist in mean grain size with TBD>TSD>TMD, sorting with TMD>TBD>TSD (larger value indicating poorer sorting), and both skewness and kurtosis with TSD>TBD>TMD. These findings will undoubtedly shed new light on our understanding of tidal-bore sedimentology, ancient tidal-bore sedimentary facies and environments, and related oil-and-gas field prospecting.

Qiantang River, tidal bore, sediment-dynamics, turbulence flow, grain-size analysis, sedimentary structure, tidal rhythmite

A tidal bore is a moving hydraulic jump, frequently occurring in macro-tidal, funnel-shaped estuaries. Tidal bores occur at over 80 river estuaries in the world [1]. The most spectacular bores are those of the Qiantang Estuary (China), the Amazon Estuary (Brazil), and the Seine Estuary (France), where the bores are rolling and breaking, and are known as breaking bores [2,3]. The massive hydraulic power of tidal bores can exert a great impact on an estuarine

*Corresponding author (email: ddfan@tongji.edu.cn)

environment, ecosystem, infrastructure, etc., and for that reason, coastal engineers pay much attention to the potential hazards of tidal bores. Over the last decade, the hydraulic behaviors of tidal bores have been extensively investigated through field observations [4–6], flume experiments [7,8], and numerical modeling [9–11]. It is generally accepted that undular bores begin to form with a Froude (F_r) number slightly above 1. As F_r increases, the stationary free-surface undulations are gradually agitated and rollers develop. Breaking bores are expected when F_r exceeds 1.7 [3,6,8,12]. A tidal bore is an intensely mixed turbulent flow. Reynolds (R_e) numbers of 8.1×10^4–11×10^4 were assigned in Chanson's modeling study of tidal bores [2], significantly above the critical R_e number of 4000 for turbulent flows. The hydraulics of the Qiantang bores has recently been studied extensively because of expanding engineering constructions in the estuary, and great advances have been achieved particularly in numerical modeling. The entire span of the bores can now be simulated from their birth, through to growth and eventual decay, and the most characteristic surface features of the bore have been successfully simulated, including the intersection and reflection of bores, and the development of straight-headed bores. The numerical modeling results have been widely employed in recent estuarine engineering design and planning projects that include harnessing river channels, reclaiming intertidal lands, and constructing cross-estuary bridges [3,13–17].

Gigantic sandbar complexes in the estuarine section are often associated with tidal bores [18,19]. A sandbar complex consisting of well sorted silts in the Qiantang Estuary is estimated to have a volume of roughly 425×10^8 m³ [19]. Spectacular tidal bores interpreted to have occurred in the Holocene Changjiang Estuary also produced a gigantic sandbar complex with a thickness of 20–30 m, composed of well sorted silts with massive bedding and erosion structures [20,21]. Buried giant sandbar complexes potentially are major reservoirs for oil and gas, so it is highly relevant to study their depositional processes and facies development. However, the present level of knowledge is still quite low regarding bore sedimentation processes and resulting sedimentary features, particularly concerning the distinguishing features of the ancient analogues. The Late Jurassic Lourinhã Formation in the Lusitanian Basin of western Portugal, could be the first report of strata bearing tidal-bore deposits; however, the authors were not confident of a tidal-bore genesis because of their lack of comparable modern analogues and a theoretical context [22]. It has basically been assumed that macrotidal embayments or estuaries were much more prevalent earlier in geological time, particularly during periods in the evolution of Pangea and Panthalassa when both nearshore and offshore tidal ranges were potentially much larger than at present [23,24]. During these times, tidal bores should have been present in some macrotidal embayments/estuaries, producing distinctive deposits. However, they may be misinterpreted as other facies rather than those related to tidal bores because of the unavailability of an appropriate facies model. For example, the sandbar complex in the Qiantang Estuary has been systematically studied since the 1960s, when Professors Ning Qian and Jiyu Chen published two cornerstone papers on the modern and historic evolution processes of the sandbar complex [18,19]. Investigations of the sedimentary and geomorphologic features of the sandbar complex have continued, e.g. studies of the complex's morphology and volume, grain-size composition and characteristic sedimentary structures [25–28]. Recent studies of strata recovered from a few boreholes penetrating through the sandbar complex show that the complex is composed of well-sorted, coarse-grain sediments, with the frequent occurrence of erosional surfaces caused by strong tidal flows at the base of sand layers [29–31]. Up to now, no systematic study of the sedimentation processes and facies of the tidal bores in the Qiantang Estuary has been undertaken.

The location of the greatest bores in the Qiantang Estuary has recently shifted from Xinwan to Daquekou, and the peak bore magnitude has increased by 0.1–0.4 m. This has occurred because the channel width has been sharply reduced following extensive land reclamation [32]. In this study, hydraulic observations were carried out at a station near Daquekou, and a few short cores were collected on the intertidal flats of Daquekou and Jianshan (Figure 1) to study sedimentary textures and structures. The aim of this work is to improve our understanding of depositional processes and develop a system of characteristic sedimentary features of the tidal bores in the Qiantang Estuary, which will be further compared with turbidites to explore the differences and similarities between tidal-bore and turbidity-current deposits, the two most-intense turbulent flows in nature.

1 Study area

Hangzhou Bay resembles a gigantic funnel, narrowing from a width of ~100 km at the bay mouth landward to less than 20 km along the Ganpu transection (Figure 1(a)). The sharp decrease in estuarine width over 80 km within a longitudinal distance of 85 km greatly deforms advancing tidal waves. In fact, the mean tidal range increases from less than 2 m at the mouth to ~5.5 m near Ganpu [33]. The bay is quite shallow with an average depth of 8–10 m at low tide, with the exception of some deep erosional channels along the northern bank. The bay morphology can be roughly divided into two parts along the Jianshanwai transection (Figure 1(a)), with relatively smooth muddy beds in the east and undular sandy beds in the west, the later characterized by alternations of tidal sand ridges and troughs together with some silty shoals [13,34,35].

The Qiantang River, which flows out into Hangzhou Bay, is highly affected by macrotides with an upstream limit of tide-induced water-level fluctuations at Lucibu, about 190 km
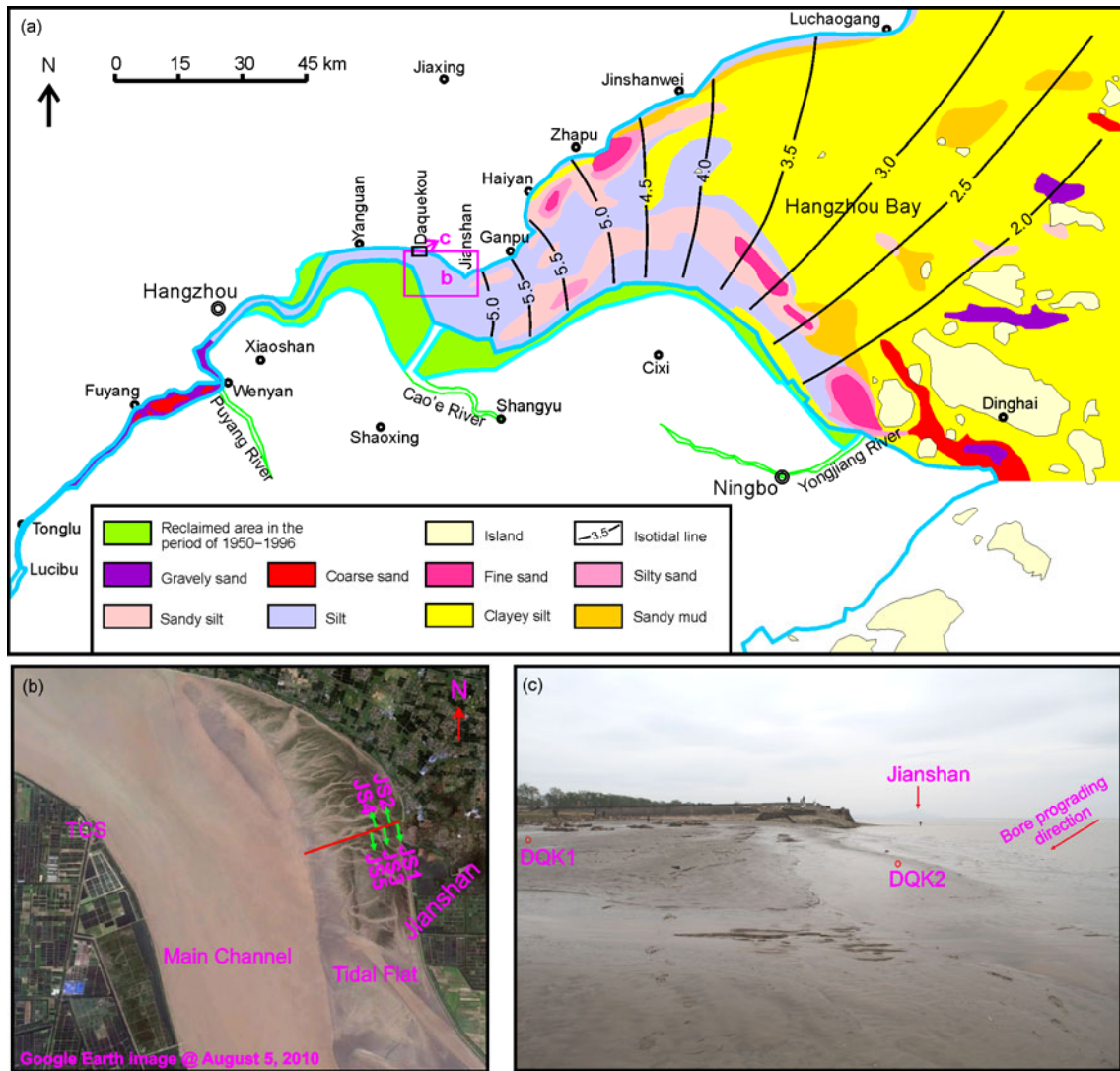
Figure 1 Maps of Hangzhou Bay and the Qiantang Estuary with the locations of field observations and sampling. (a) Changes in mean tidal ranges and the surface sediment composition within the bay and estuary (modified from [24,29,34]); (b) locations of short cores overlaid on a Google Earth satellite map of the Jianshan intertidal flats; (c) locations of short cores on the Daquekou intertidal flats.

upstream from Ganpu (Figure 1(a)). Bores are usually initiated in the region of Ganpu to Gaoyangshan during spring tides, growing upstream and reaching their peaks near Daquekou. Upstream of here, the bores decay and finally disappear a little upstream of Wenyan. The estuarine section with tidal bores is roughly 90 km long, characterized by the intense interaction of river flows and tides in the broad and shallow channels above the gigantic sand-bar complex. The estuarine channels shift frequently because of erosion and the predominance of coarse silts. The lower reach of the river, extending over 75 km from Wenyan to Lucibu, is fluvially dominated with significant water-level fluctuations caused by tides. The channel sediment here is dominated by sandy gravels or gravely sands [3,5,13,29].

The sandbar complex in the Qiantang Estuary has a lenticular shape, with a longitudinal (east-west) length of ~130 km, and a transectional (north-south) width of ~27 km (much

wider than the present river channel), and a maximum thickness of 10–20 m. The total volume is estimated at over 425×10^8 m^3 [19]. The complex has its topographic vertex between Cangqian and Qibao. The elevation here is roughly 10 m above the baseline linking the bed tops at Zhapu and Wenyan with a very gentle seaward-sloping gradient of 0.02% [5,19,36]. Mid-channel bars and intertidal flats are extensively developed in the estuarine section with significant erosional/depositional cycles; most of these bars have been reclaimed since the 1960s. The Jianshan intertidal flats constitute the largest bank in the estuary, with a maximum width of 2.5 km and a total area of >25 km^2 (Figure 1(b)). The Daquekou intertidal flats, which have developed between two headlands, are ~500 m long and ~100 m wide with a relatively steep slope of 1/20. They are intensely shaped by the straight strikes of advancing bores with surges and currents washing up and down the slope (Figure 1(c)).

2 Methods

2.1 Field observations and short-core sediments sampling

Field observations were carried out at the Daquekou water-level gauging station during spring tides in the period from April 30 to May 2, 2010 (Table 1). At the test site, a high scaled rod was firmly erected above the riverbed at a distance of ~50 m from the riverbank. Two optical backscatter sensors with conductivity, temperature and depth detectors (OBS-3A from the D&A Company of the USA) were fixed directly along the gauging rod, with lower and upper detectors located about 1 and 1.7 m above the river bed. The position of the lower detector was close to the low-tide level during the deployment. One 1200 kHz acoustic Doppler current profiler (ADCP from the RDI Company of the USA) was fixed on the river bed by a steel frame with the detector about 50 cm above the bed; the ADCP was set looking upward with 10 cm bins and a 10 s sampling interval.

Short cores were sampled completely by hand. First, 50–70 cm long PVC tubes were hammered into the intertidal deposits, then dug out using shovels. The core sediment samples were then firmly sealed and taken back to the laboratory for further analyses. Five short cores were extracted from the middle transection of the Jianshan intertidal flats (Figure 1(b)), and two short cores from the top and bottom of the Daquekou intertidal flats (Figure 1(c)). Details of the sampling locations are listed in Table 1.

2.2 Core logging and grain-size analyses

Each sediment core was split in half at the laboratory, and the archived halves were sealed with preservative film and sent for storage to a low-temperature (usually 4°C) core repository. The sediment surface of the working halves was carefully scratched by steel knives to show clear sedimentary features on a flat plane. Following this, photos were taken and the cores were logged to record such information as sediment color, grain size composition and characteristic sedimentary structures. To make a detailed examination of

the products of different tidal processes, all sediment samples for grain-size analyses were carefully taken within single sandy/muddy layers with small sampling locations at scales of 2×2 mm^2 – 3×3 mm^2. Some thick sandy beds were continuously sampled at an interval of 2 cm. There were a total of 255 sediment samples collected from seven short cores, and the sampling spots were directly marked on the graphical core sections (Figure 2). Each sample was weighed at 0.25–0.35 g for muddy deposits, and 0.45–0.55 g for sandy deposits.

All sediment samples were pretreated with the methods described in detail by Guo et al. [37] before instrumental measuring, including a treatment with 10% diluted hydrochloric acid and 30% oxydol to remove carbonate and organic matters respectively. The sediment-suspension samples were repeatedly washed with deionized water to neutral, and then dispersed for a few minutes in an ultrasonic vibrator before measuring using the laser-diffraction size analyzer of Beckman Coulter LS230, with a detection range of 0.375–2000 μm.

Grain-size parameters were calculated with the moment method, and C (the one percentile size) and M (the median diameter) values were computed using the cubic interpolation method of Matlab.

3 Results and discussions

3.1 Tidal surge, flood and ebb processes

One ADCP was deployed on the morning of May 1, 2010, and retrieved after two semi-diurnal tides. Current data from the first tidal cycle were determined to be of high quality, meriting further study. Data from the lower OBS were presumably reliable during the deployment period from the afternoon of April 30 to the morning of May 2, 2010. Therefore, the instrumental data from the overlapping period were selected to study the change in water level, current velocities, and turbidities within a tidal cycle during a spring tide, specifically from 13:29 to 19:00 on May 1 and from 13:27 (2 min ahead of the bore arrival) on May

Table 1 Locations of hydraulic observations and short cores sampling, length of the cores and number of sediment samples taken for grain-size analyses

Sections	Stations	Longitude (E)	Latitude (N)	Length of cores (cm)	Number of samples for grain-size analyses
Daquekou	Hydraulic station	120°39′29″	30°34′26″	–	–
	DQK1	120°39′45″	30°24′03″	48.5	31
	DQK2	120°39′44″	30°24′01″	63	27
Jianshan	JS1	120°44′30″	30°21′38″	52	59
	JS2	120°44′23″	30°21′36″	55	44
	JS3	120°44′16″	30°21′34″	58	34
	JS4	120°44′09″	30°21′32″	56	30
	JS5	120°44′02″	30°21′30″	59	30
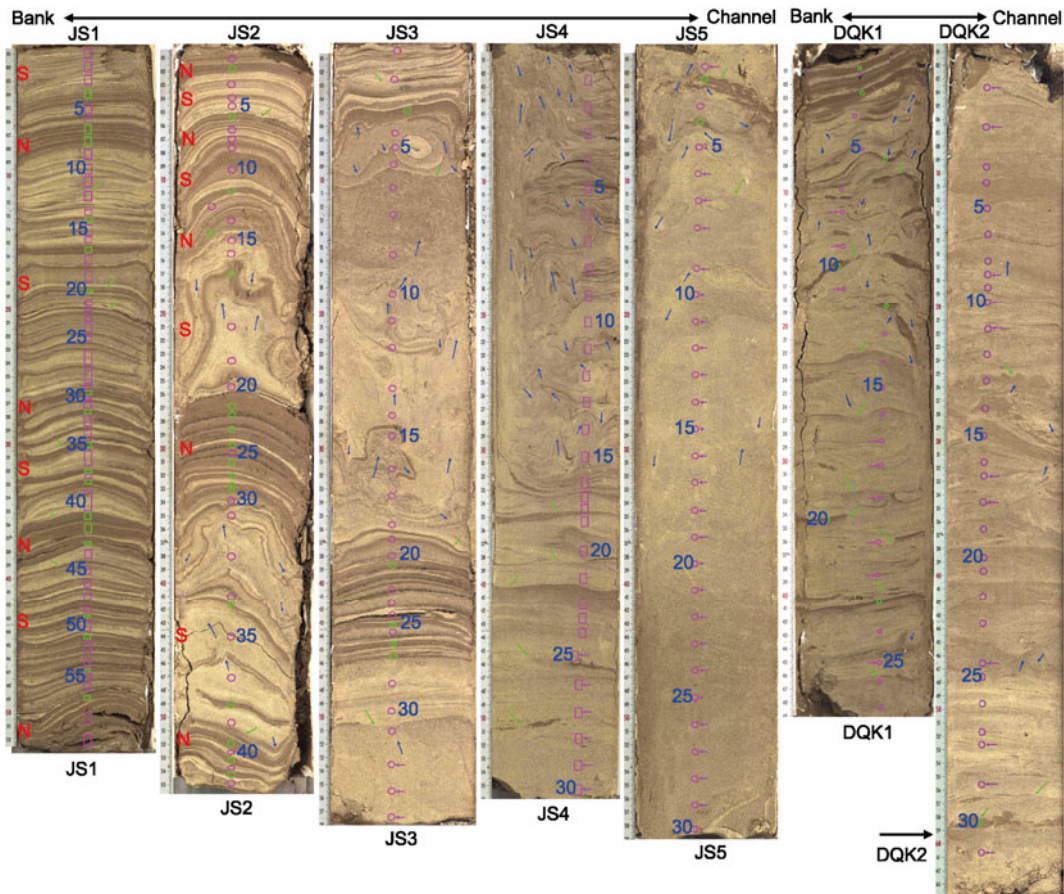
Figure 2 Photographs of short cores with sampling locations and characteristic sedimentary structures indicated (JS1–JS5, DQK1, DQK2). Green and pink circles or squares denote the sampling locations on muddy and sandy layers, respectively, with sample numbers marked nearby; horizontal pink arrows denote tidal-bore depositional layers; green and blue arrows point to scour structures and water-escape structures, respectively; S and N represent the spring and the neap tides, respectively.

1 to 2:00 on May 2 (immediately after the second bore to rapid flooding stage). Water-level and turbidity data were plotted every minute (Figure 3(a)). The current velocities in the direction of the main channel were calculated from the primary current data by using the vector combination method with positive and negative denoting flood and ebb flows, respectively. The deduced current data were plotted every 10 min (Figure 3(b)), except for the first 10 min when they were plotted every minute to show clearly the sharp variations in velocities.

The asymmetry between the flooding and ebbing durations is highly evident near Daquekou, with very short flooding periods of roughly 2 h and relatively long ebbing periods lasting over 2 h. The transition from the flood to ebb flow occurs 30–60 min after the high tide with the velocity approaching to zero. One single tidal cycle can be divided into 7 stages on the basis of characteristic variations in water levels, flow velocities and turbidities (Figure 3).

(1) Bore to rapid flooding stage. This lasted for merely ~20 min with the first several seconds of the bore-head passage characterized by significant breakers and rollers, followed by rapid flood flows with velocities that changed between 1.10–2.10 m/s with an instantaneous maximum speed of 2.47 m/s. The water level was elevated abruptly by ~2 m during the bore-head passage, and continued growing higher rapidly throughout the stage. The turbidity rose rapidly from near zero to 1800 NTU in the 5 min after the passage of the bore, and then fluctuated in the range of 1800–2000 NTU.

(2) Sharply decelerated flooding stage. This period was characterized by an abrupt decrease in velocity from ~1.10 to ~0.60 m/s, and turbidity from ~1800 to ~450 NTU over 30 min, while the water level still rose at a relatively rapid speed.

(3) Slow flooding stage. The velocity dropped rapidly below 0.50 m/s in the early stage and then stabilized at between 0.15 and 0.30 m/s for a longer time. The turbidity declined slowly toward a minimum value of ~170 NTU over the whole flooding period. The water level rose slowly toward its highest point and then declined very slowly for a few centimeters during the late stage.

(4) Transitional stage. The velocity approached zero. The water level began slowly descending, and the turbidity fluctuated but with a small ascending trend.
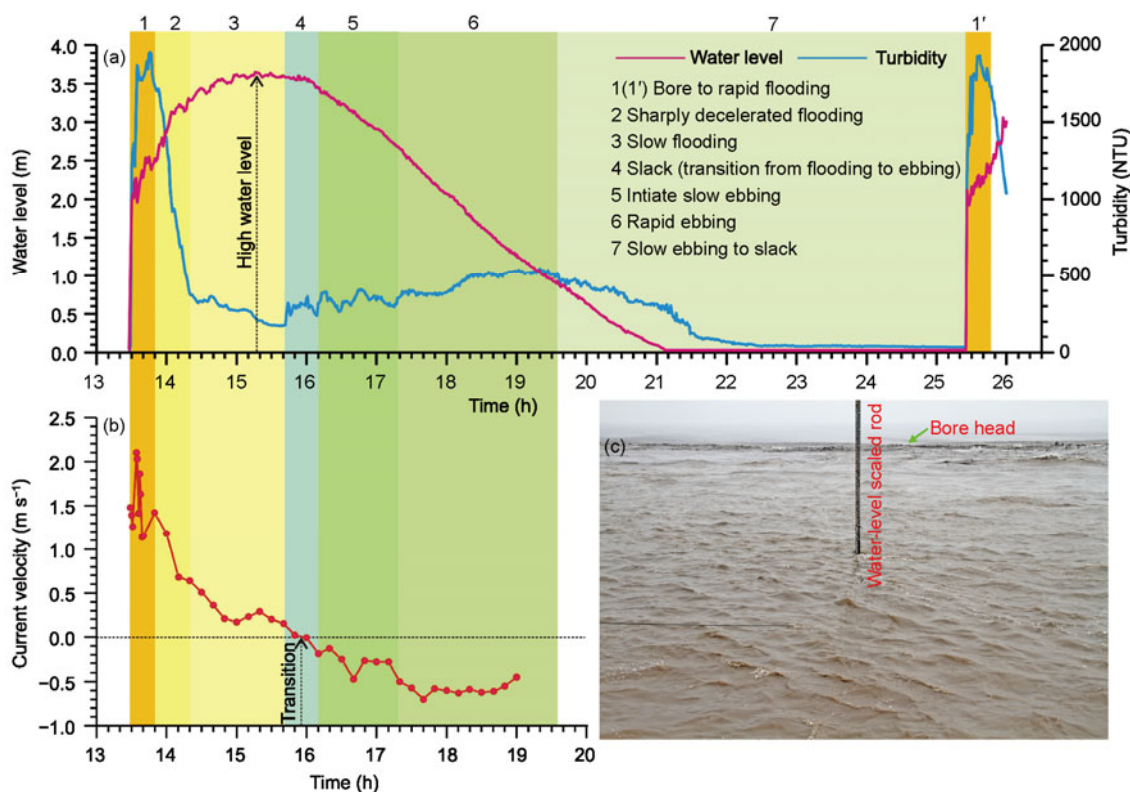
Figure 3 Changes in water level stages, turbidities (a), and tidal flows (b, positive denoting flood flows), within a tidal cycle during a spring tide at the Daquekou gauging station in the Qiantang Estuary. The photo shows the rolling bore head and highly turbid water behind the bore, taken at 12:53 on April 30, 2010 (c).

(5) Initial slow ebbing stage. Both the velocity and the turbidity were slowly increased with evident undulations. The water level declined relatively rapidly.

(6) Rapid ebbing stage. The velocity stayed above 0.50 m/s for a long time before declining at the late stage. The turbidity increased slowly toward a maximum of ~550 NTU before decreasing during the last ten minutes. The water level fell relatively rapidly.

(7) Slow ebbing to slack stage. No current data were available because of subaerial exposure of the ADCP during the low tide. The flow was visually observed to be very slow and the water level declined relatively rapidly to the low tide at the early stage and then remained for ~4 h while the tide was slack. The turbidity dropped rapidly from ~500 to ~100 NTU during the first 2 h, and then decreased slowly toward and fluctuated near 30–40 NTU until the arrival of the next bore.

3.2   Sedimentary structures

Various sedimentary structures are well developed in the short-core sections (Figure 2, Table 2). Primary structures typical of a tidal genesis include mud drapes, mud couplets, spring-neap tidal cycles, and bi-directional cross-laminae. These occur widely in cores DQK1 from the Daquekou upper intertidal flats, and JS1–JS3 (typically JS1) from the

Jinshan upper intertidal flats. Sedimentary structures like ripple beddings, inclined and parallel beddings are interpreted to have formed under increasing energy conditions according to their characters and development locations. For example, ripple beddings are widely present at the top of JS3 without the direct impact of tidal bores, whereas inclined and parallel beddings are evident in the two cores from the Daquekou intertidal flats and the lower part of JS4, which were highly exposed to the direct influence of tidal bores. Scour structures are extensively distributed in all cores, particularly at the base of thick sandy laminae or massive sand beds, indicating their genesis by the eroding forces of strong tidal flows near the bank and of tidal bores near the main channel. Well-compacted massive beddings are evident in the cores taken from the middle-to-lower intertidal flats at Jianshan, where JS5 is almost completely composed of massive beddings, with the exception of the topmost 6.5 cm; massive beddings are only present in the lower parts of JS4 and JS3. We therefore suggest that massive beddings are the result of rapid deposition after the bore to rapid flooding stage.

Water-escape structures and associated secondary structures like folded and convoluted beddings are also widely present in the cores (Figure 2, Table 2). They are particularly evident in cores JS3, JS4 and DQK1, where abundant dark platy minerals are arranged regularly into laminae in

Table 2 Characteristic sedimentary structures and interpretations of their genesis

Type	Nomenclature	Distribution	Genesis interpretation	
Primary sedimentary structures	Muddy drapes or laminae	Present on all cores, typically well developed on JS1, common on JS2, JS3, and DQK1, scare on the others	Deposition by slow flows approaching or at the slack tides	Regular tidal flows
	Mud couplets	Present on JS1 and JS2, typically at the section of 42–45 cm on JS1	Two thin muddy laminae formed during the slack tides, with one intercalated sandy lamina by the weak ebb flow	
	Spring-neap tidal cycles	Distributed on JS1, JS2, and JS3, typical for those on JS1	Thicker and thinner sandy laminae formed respectively at spring and neap tides, cyclic changes in lamina thickness denoting the spring-neap tidal cycles	
	Ripple beddings	Typical at the topmost 3 cm of JS3	Production of lateral progradation of small current ripples	
	Parallel and inclined beddings, bi-directional cross beddings	Majorly present on JS4, DQK1, and DQK2	Production of bi-directional tidal flows, lateral progradation of current ripples, or aggradation over the plane bed	
	Scour structures	Extensive distribution on all cores, typically at the base of thick sand laminae or massive sand beds	Result of erosion by strong tidal flows	Strong tidal flows
	Massive beddings	Typically on JS5 except the topmost 6.5 cm, and the lower ports of JS3, JS4	Coarse-grained, massive beds denoting rapid deposition after the bore to rapid flowing regime	
Secondary sedimentary structures	Dewatering structures	Widely present in all cores except JS1, typical for those on JS3, JS4, and the upper section of DQK1	Some downward folded laminae potentially produced by the direct response to great pressure of the surging head	Tidal bores
	Folded and convoluted beddings	Commonly present together with dewatering structures	Primary structures deformed by liquefaction and dewatering	
	Load, fault and sliding structures	Common on JS4, JS5, DQK1, and DQK2	Product of gravity action and sand layer liquefaction	

the thick sand beds. Together with mud drapes at the top, they act as barriers to the agitating pore water at the initiation stage of liquefaction. Eventually, they were breached as the power-water pressure increased to produce dewatering pipes, and convoluted and folded beddings. The overpressurization of sandy layers is interpreted to have resulted mainly from the abrupt increase in water level and the intense beating of the breakers and the rollers during the passage of tidal bores. Some downward folded laminae or deformed structures are presumably a direct response to the intense surging pressure at the early stage. Then, upward oriented dewatering structures were produced when the top pressure decreased after the passage of a tidal bore. Small fault and sliding structures are widely distributed in DQK1 and DQK2, potentially resulting from the joint action of gravity, intense bore surging and back-washing currents on the steep bank.

3.3 Grain size analyses

(i) Grain size compositions and parameters. Deposits in the short cores from the Jianshan and Daquekou intertidal flats are mainly composed of silts. The mean grain sizes are 5.04 φ and 6.04 φ respectively for sandy and muddy laminae/beds with predominant compositions of very fine sands to coarse silts and medium to fine silts (Table 3). The sorting (standard deviation) values fluctuate over a small range from 1.33 φ to 1.86 φ, denoting poor sorting based on the model of Jia et al. [38] for the moment parameters. The sorting of the sandy layers is generally a little better than

that of the muddy layers, although their difference is quite limited. The skewness values change over a wide range from 0.29 to 2.44, supposing positive to strongly positive skewness, a common feature for tidal deposits having a tail of excess fine particles that are deposited during times of slack tides. The mean skewness values are 1.09 (positively skewed) and 1.94 (strongly positively skewed), respectively, for the muddy and sandy layers. The difference is mainly attributed to their different grain size compositions, especially the predominant size components. Additional inputs of extremely fine particles form a long fine-grain tail to the coarse-grain predominance of the sandy layers, while they have little effect on those dominated by fine grain sizes, i.e. muddy layers. Grain-size frequency curves are all generally single-crested, and the kurtosis values change from 2.31 to 8.99, which ranks as leptokurtic to very leptokurtic magnitudes. The mean kurtosis value (6.70) for the sandy layers is almost double that of the muddy layers (3.70), which corresponds to the former having better sorting and higher concentrations of the predominant grain sizes than the latter.

Grain-size analyses of the sand layers show a general fining-bankward trend on the Jianshan intertidal flats, with a bankward decrease in sand contents vs. increase in silt contents (Table 3), determined by the gradual weakening of tidal flows in the same direction. However, the difference is not significant between DQK1 and DQK2 in terms of size percentages and size parameters (Table 3), even though they were extracted near the top and the bottom of the Daquekou intertidal flats, respectively. This is assumed to be the result of intense mixing by strong tidal surging, upward and

Table 3 Grain size parameters of the Jianshan and Daquekou intertidal deposits

Sandy/muddy layers		Numbers of samples	Mean size (φ)	Sorting (φ)	Skewness	Kurtosis	Sediment size percentages		
							Sand	Silt	Clay
Muddy		50	6.04	1.65	1.09	3.70	3.14	82.04	14.82
Sandy		205	5.04	1.49	1.94	6.70	16.54	76.37	7.09
Sandy	JS1	42	5.23	1.46	1.88	6.45	8.70	83.75	7.55
	JS2	26	5.34	1.48	1.82	6.12	7.68	83.97	8.35
	JS3	29	5.00	1.46	1.95	6.90	16.11	77.28	6.61
	JS4	30	4.98	1.44	2.11	7.48	16.37	77.19	6.44
	JS5	28	4.73	1.58	1.89	6.39	33.37	59.94	6.69
	DQK1	20	4.91	1.48	2.06	7.11	20.25	73.17	6.58
	DQK2	30	4.98	1.51	1.93	6.60	17.61	75.22	7.16

backward swashing over the entire narrow intertidal zone, making it difficult to deposit fine grains any higher on the higher intertidal flats. Note that the parameters of sorting, skewness and kurtosis do not vary significantly in the sandy layers of the various cores (Table 3).

(ii) Discrimination between tidal-bore and regular-tidal deposits. Scattering plots of two different grain-size parameters have been used widely to discriminate between different major sedimentary environments. They are employed here to study different tidal depositional processes and their related products. The bivariate plot of mean grain size and sorting displays a general shape "√" for all samples from the Jianshan intertidal flats, with muddy deposits concentrated in the upper-right area and sandy deposits in the lower-left (Figure 4(a)). Detailed comparison studies between sedimentary structures and grain-size characters found that the sampled sandy sediments exhibited a tidal bore genesis based on the sedimentary structures like thick massive beddings are concentrated at the upper-left region, and other sandy samples are assembled at the lower-central region. The sandy deposits can be further subdivided into those with a bore genesis at the upper left and those with a regular tidal genesis at the lower central (Figure 4(a)). The sandy layers in the Daquekou intertidal flats are difficult to characterize as bore or regular tidal deposits based simply on the sedimentary structures, because massive beddings are absent or not well developed. These grain-size data were plotted on an interpretative map of depositional processes at work in the Jianshan intertidal deposits. This shows that the muddy-deposit samples were mostly concentrated in the tidal muddy deposit (TMD) areas. Some sandy-deposit samples were plotted in the tidal sandy deposit (TSD) areas and others were interpreted to be in tidal bore deposit (TBD) areas (Figure 4(b)). All tidal-bore-deposit sampling locations that could discriminate relationships between mean grain size and sorting were directly marked on the core sections (Figure 2). Most of these samples have been demonstrated to have come from the basal parts of sandy layers with well developed massive beddings, parallel or inclined beddings, supporting their production as part of a

high-energy tidal process. It is therefore concluded that TMD, TSD and TBD can effectively be discriminated through the use of a bivariate plot, between mean grain size and sorting, because of the different mechanisms of tidal deposition that they follow.

Bivariate plots of sorting vs. skewness or kurtosis also demonstrate the different distribution patterns of TBD, TSD and TMD. Their distributions can be easily discriminated with clear boundaries among the three kinds of tidal deposits on the Jianshan intertidal flats. The linear regression analyses show high but negative relationships of sorting vs. skewness or kurtosis for each tidal depositional subdivisions with the least R^2 value equal to 0.755 (Figure 4(c),(d)).

(iii) *C-M* diagram and its interpretation. The general *C-M* distribution pattern of seven short cores from the Jianshan and Daquekou intertidal flats is quite similar within the segments of S-R-Q-P in the fluvial *C-M* diagram [39] (Figure 5). The *C-M* points of TMD scatter over a wide range, but the major components occupy the SR segment, parallel to the *X*-coordinate (*M* value), representing sediments transported as a uniform suspension. The TSD and TBD *C-M* points are mostly distributed at the lower and upper parts of the RQ segment, respectively, with some TBD *C-M* points scattering at the PQ segment. The RQ segment, which is characterized by being parallel to line *C=M*, denotes sediments transported as a graded suspension. The PQ segment, characterized by being of parallel to the *Y*-axis (*C* value), represents sediments transported mainly in a graded suspension with some in a rolling component. In short, sediments in the section of the Qiantang Estuary affected by the bore mainly were transported as suspended load, with a small fraction, if any, transported as bed load.

Some small areas of overlap do exist between TBD and TSD, and TSD and TMD in the *C-M* diagram. This indicates the gradual transition among the three different depositional processes. The values of Cu and Cs, corresponding to the largest grain size transported as a uniform suspension and a graded suspension, are 90 μm (3.5 φ) and 165 μm (2.6 φ), respectively. These values are both lower than those found
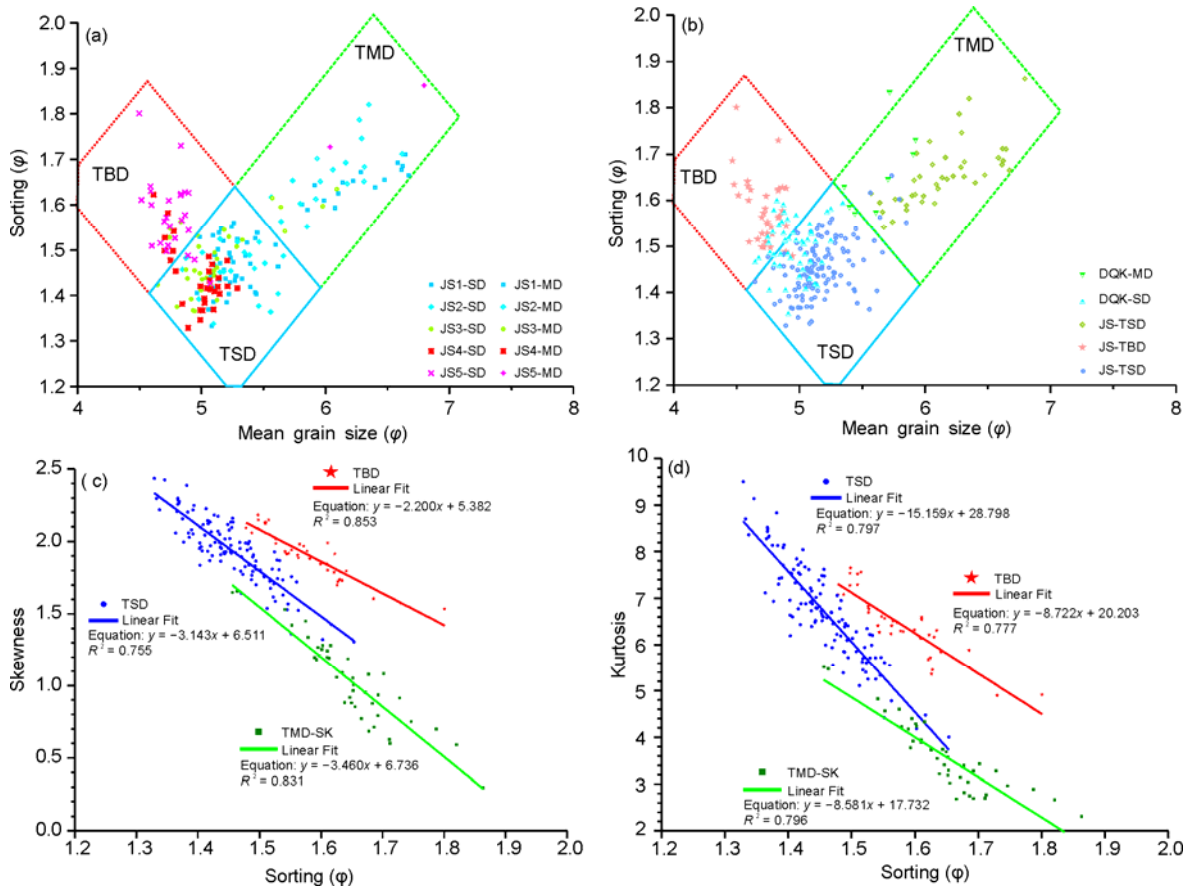
Figure 4 Grain-size bivariate plots of mean grain size vs. sorting ((a), (b)), and sorting vs. skewness and kurtosis ((c), (d)). TBD is abbreviation for tidal bore deposits, TSD for tidal sandy deposits, TMD for tidal muddy deposits, SD and MD for sandy and muddy deposits.
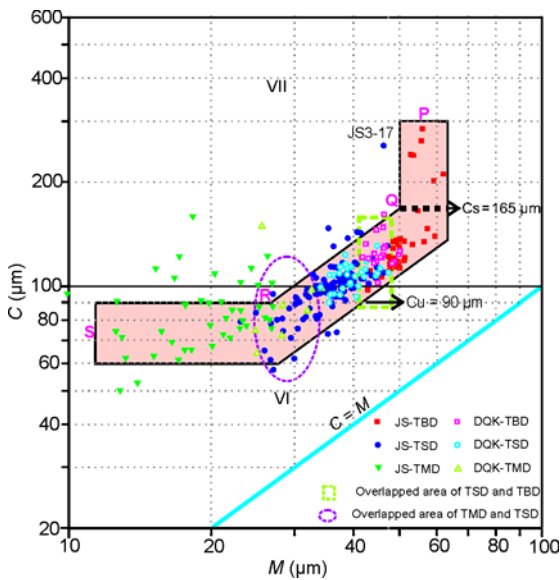
Figure 5 *C-M* diagram of tidal deposits along the north bank of the Qiantang Estuary affected by tidal bores.

3.4 Mechanisms of tidal bore sedimentation and the formation of their characteristic sedimentary structures

The asymmetry between the flooding and ebbing phases of tides in the Qiantang Estuary is extraordinary. This is assumed to be the major mechanism controlling sediment suspension, transportation and deposition in the section of the river affected by the bore. The ebb duration is generally several times longer than the flood duration [3,13]. For example, an ebb duration of more than 10 h is approximately four times the flood duration of more than 2 h observed during the spring tides at Daquekou. The maximum near-bottom (1 m above the bed) velocities for this period were 0.7 and 2.1 m/s for the ebb and flood flows, respectively, with the latter being three times the former. The maximum turbidity variation usually occurs at the same moment as the passage of the bore-head, and a few minutes ahead of the maximum flooding regime. The hydraulic observations at Daquekou showed that the suspended concentration jumped sharply from a minimum value in the range of 0–50 to 1300–1800 NTU within one or two minutes before and after the bore. Another field observation at the Twentieth Construction Section (TCS or Ershigongduan), opposite Daquekou (Figure 1(b)), also showed the same phenomenon

in fluvial deposits [39], which is potentially controlled by the major component of fine grains in the Qiantang Estuary, which has very few grains coarser than coarse silts.

with an abrupt increase in turbidity from ~0 to 70 g/L immediately before and after the bore [16]. It was thus extrapolated that vast amounts of sediment resuspension was mainly ascribed to the intense turbulence and mixing of breaking and rolling waves at the bore head.

Both flume experiments and numerical modeling results demonstrate that the eddy turbulence generated by tidal bores, typically by breaking bores with R_e higher than 10^4 [2], was highly capable of eroding and suspending huge volumes of sediment. Sediment dispersal is highly determined by tidal flows. Rapid flood flows following the passage of the bore potentially transport vast amounts of sediment upstream and toward the intertidal flats during a stage with high suspended-sediment concentrations and rising water level. During the following stage, vast amounts of suspended sediments should be deposited rapidly because of a sharp deceleration of flood flows. This lasted only 30 minutes with a drastic drop of turbidity from ~1800 to ~450 NTU according to our single field observation. After these first two stages, absolute values of flow speeds and their variation magnitudes were relatively small. A maximum speed of 0.7 m/s occurred at the rapid ebbing stage, but its general competence to resuspend sediments was presumably low and the suspended sediment concentration was not observed to increase significantly either. The suspended sediment concentration fluctuated between 300 and 500 NTU for a long time following the slow flooding stage (stage 3), and declined toward zero from the late slow ebbing stage to the slack stage (stage 7, Figure 3). In short, sedimentation in the bore-affected section of the river is mainly controlled by the tidal bore and closely related processes, including the abrupt rise in water level, and the rapid increase and decrease in flow velocities during and immediately after the passing of the tidal bore. Although all these processes only account for roughly one tenth of a single tidal cycle, and regular tidal processes over the remaining nine tenth of the tidal cycles have a limited capacity to affect bed morphology and strata formation, especially for the main channel.

In the river section of the Qiantang bore, the deposits are mainly composed of coarse silts and fine sands with a phi value between 2 and 5 φ, characterized by easy resuspension and resettling [5,13]. The main channel deposits consist of 70%–80% coarse silts and fine sands with very few grains coarser than coarse sand, so almost all sediment is subject to resuspension by the intense erosion and eddy turbulence of the breaking bores. This conclusion is supported further by the *C-M* graphic interpretation. Where most *C-M* points accumulate on the SR and RQ segments, representing sediments transported as uniform suspension or graded suspension, and only a few points fall on the PQ segment that denotes the predominance of suspended loads over bed load. Absolutely no points are plotted on the OP and NO segments that represent the dominance of bed load (Figure 5). We postulate that the suspended sediments were fully mixed to form uniform suspension under intense vor-

tex turbulence at the bore to rapid flooding stage. Rapid sedimentation of these suspended sediments should then occur at the sharply decelerating flooding stage, which corresponds to decreased turbulence. Settling sediments potentially increase the suspended concentration near the bottom, leading to stratification, which further depresses the turbulence and promotes sedimentation [39]. Coarse sediments should be first to settle out of the water to deposit massive bedding, graded bedding, etc., and produce characteristic structures that can be used to discriminate tidal bore deposits from other types of deposits (Figure 2). Although tidal bore deposits are the product of high-energy flow, their sorting is usually poor because of rapid deposition from a highly mixed suspension. At the slow flooding stage, lower rates of sedimentation occur because of lower suspended sediment concentrations. Stable flow conditions favor the development of well sorted strata, even though the currents are still high enough to transport coarse grains as graded suspension. Increasing bed loads then deposit to form parallel bedding, ripple bedding and bidirectional cross-bedding. During the transitional stage from flooding to ebbing with the current velocity approaching to zero, the high tide potentially lets the upper uniform suspension flow over the upper intertidal flats to deposit fine-grain layers that are predominantly muddy and poorly sorted. The characteristic sedimentary structures observed in the five short cores from the Jianshan intertidal flats reveal the depositional trend of three tidal processes from sharply decelerating, through slow flooding, to the a transitional stages, where the tidal bore deposits mainly occurred in the main channel and the middle-lower intertidal flats, and tidal sandy and muddy deposits were mostly deposited and preserved at the middle-upper intertidal flats as water level subsequently rose and the velocity of flows decreased (Figure 2). The *C-M* points were plotted in separate segments from PQ to QR to RS, denoting the direction of energy decrease for the three different depositional processes. The sediment dynamics are significantly different among TBD, TSD and TMD thereby producing diverse grain-size compositions that potentially can be characterized using bivariate plots of any two grain-size parameters (Figure 4).

The ebb flows in the Qiantang Estuary are generally weak at the intertidal flats, with limited effect on sediment resuspension, transport and deposition to produce or preserve individually discernible sedimentary units. However, the ebb flows are relatively enhanced during spring tides, and can produce competent deposits of a few millimeters in thickness. These are usually manifested as 1–2 mm thick sandy laminae at the middle-upper intertidal flats, which are interlayered with two muddy laminae to form mud couplets (Figure 2). Such couplets are extensively used as a discrimination marker for tidal deposits. The groupings with thicker sandy laminae and well-developed mud couplets in JS1 were therefore interpreted to be spring tide deposits, whereas groupings with thicker muddy laminae and a lack of mud

couplets were assumed to be neap tide deposits; their alternations therefore denote spring-neap tidal cycles. The rhythmic deposition of spring-neap tidal cycles may be a common accompaniment of tidal bores, usually developing at the middle-upper intertidal flats or at the flanks of small creeks where direct strikes of the tidal bores do not occur (e.g. the Turnagain Arm Estuary, Alaska [40]).

The riverbed of the Qiantang Estuary is subjected to serious erosion and sediment suspension under the joint actions of strong tidal flows, the intense pressure of tidal surges, breaking and rolling waves, and vortex turbulence. These processes result in various scour structures in the strata. New depositional beds have a high potential to liquefy under sharply increased pressure from abruptly rising water levels combined with breaking and rolling tidal surges, creating various convoluted bedding and dewatering structures. The pressure exerted by the passage of tidal bores was measured to reach 70 kPa in the Qiantang Estuary [13], potentially causing the new rapidly deposited beds containing abundant pore water to liquefy. Some downward folded beddings at the basal part of deformed sand layers are assumed to have resulted from the direct impact of the bore. As the top pressure by the external forcing decreases and is exceeded by the internal pressure of the roiling pore water because of liquefaction, normal dewatering structures are formed with upward folded or convoluted bedding (Figure 2). For example, soft-sediment deformation structures and small dewatering pipes are commonly reported in the intertidal depositional strata of the Turnagain Arm Estuary. These were originally ascribed to seismic events in this intense earthquake prone region, but following detailed field observations are now considered to have formed by tidal bores [41].

Eddy turbulence originating from tidal bores is highly similar to that related to turbidity currents. The deposits that they produce share some common features, like poor sorting due to rapid deposition, and the development of massive bedding, graded bedding, scour structures, convolute bedding and dewatering structures [42]. They are, however, obviously different in their environment of deposition and flow regimes. A turbidity current is a type of sediment gravity flow that forms mainly in a deep-water environment; a tidal bore is produced by the deformation of an advancing tidal wave in a shallow water environment. Tidal-bore deposits in main channels grade laterally to regular tidal deposits, with characteristic tidal beddings found in higher and shallow tidal flats. Therefore, it is easy to discriminate tidal-bore deposits from turbidites in terms of their associations with neighboring facies in a sedimentary system.

4 Conclusions

A tidal bore is a unique geological process on the Earth's surface that creates characteristic sedimentary morphologies and strata. A tidal bore can be a highly powerful agent when it triggers a sharp increase in water level, flow speeds, suspended sediment concentration, and impulse forcing during the passage of breaking and rolling bore heads. Breaking bores and subsequent rapid flows have many similarities with turbidity currents in terms of upper-flow regime ($F_r > 1.0$) and intense turbulent flow ($R_e > 10^4$) observed with maximum velocities of several meters per second. Rapid sedimentation occurs at the sharply decelerated flooding stage, producing poorly sorted deposits characterized by massive bedding, graded bedding and basal scour structures. Soft-sediment deformation structures are also developed, including convoluted bedding and dewatering structures. These occur because of the liquefaction of newly deposited beds that contain abundant pore water, triggered by the passage of the bore above. The *C-M* graphic interpretation demonstrates that the sediments are mainly transported as suspended loads with only a slight amount of bed load under fierce vortex turbulence in the bore-affected river section. The sedimentary features of tidal-bore deposits are highly similar to those observed with turbidites. However, in obvious contrast from turbidity currents of sediment gravity flows, tidal bores occur at the highly deformed front of advancing tidal waves as they propagate into a shallow and funnel-shaped estuary. The tidal bore and subsequent rapid flood flows take a leading role in shaping estuarine morphology and depositional strata, even though they only account for about one tenth of a single semidiurnal tidal cycle. Regular tidal flows over the remaining nine tenths of the tidal cycle exert high impacts on sedimentation at the higher intertidal flats. Tidal-bore deposits therefore can be discriminated from other rapid deposit events in terms of their facies association with regular tidal deposits at the top and on both flanks. The differences between tidal-bore and regular tidal deposits are evident not only in sedimentary structures, with the former having characteristic thick massive beddings and the latter commonly developing with tidal beddings (lenticular, wavy and flaser beddings), mud couplets, and spring-neap tidal cycles, but also in the grain size composition. Scattering plots of any two grain-size parameters have the potential to differentiate the three kinds of tidal deposition: TBD (tidal bore deposit), TSD (tidal sandy deposits) and TMD (tidal muddy deposit), with some general trends in terms of mean grain size with TBD>TSD>TMD, sorting of TMD>TBD>TSD (larger value indicating poorer sorting), and both skewness and kurtosis with TSD>TBD> TMD.

1   Bartsch-Winkler S, Lynch D K. Catalog of worldwide tidal bore occurrences and characteristics. US Geol Survey Circ, 1988, 1022: 1–17

2   Chanson H. Current knowledge in hydraulic jumps and related phenomena: A survey of experimental results. Eur J Mech B-Fluid, 2009, 28: 191–210

3   Lin B Y. Characters of Qiantang Bores (in Chinese). Beijing: Ocean Press, 2008

4   Wolanski E, Moore K, Spagnol S, et al. Rapid, human-induced siltation of the macro-tidal Ord river estuary, western Australia. Estuar Coast Shelf S, 2001, 53: 717–732

5   Lin B Y, Huang S C, Mao X Z, et al. Deformation process of tidal waves in the Qiantang Estuary (in Chinese). J Hydrodynam, 2002, 17: 665–675

6   Chen S L, Gu G C, Liu Y S. Formation conditions and initial site of tidal bores in the north branch of the Yangtze Estuary (in Chinese). Shuili Xuebao, 2003, (11): 30–36

7   Donnelly C, Chanson H. Environmental impacts of undular tidal bores in tropical rivers. Environ Fluid Mech, 2005, 5: 481–494

8   Koch C, Chanson H. Turbulent mixing beneath an undular bore front. J Coast Res, 2008, 24: 999–1007

9   Madsen P A, Simonsen H J, Pan C H. Numerical simulation of tidal bores and hydraulic jumps. Coast Eng, 2005, 52: 409–433

10 Pan C H, Lin B Y, Mao X Z. 2D numerical simulation of tidal bore in the Qiantang River (in Chinese). Ocean Eng, 2007, 25: 50–56

11 Lubin P, Glockner S, Chanson H. Numerical simulation of a weak breaking tidal bore. Mech Res Commun, 2010, 37: 119–121

12 Lin B Y, Huang S C, Mao X Z. Analyses of undular hydraulic jump and undular bore (in Chinese). J Hydrodynam, 1998, 13: 106–115

13 Han Z C, Dai Z H, Li G B. Regulation and Exploitation of the Qiantang Estuary (in Chinese). Beijing: China Water Power Press, 2003

14 Pan C H, Lu H Y, Zeng J. Characteristic and numerical simulation of tidal bore in the Qiantang River (in Chinese). Hydro-Sci Eng, 2008, (2): 1–9

15 Pan C H, Lin B Y, Mao X Z. Case study: Numerical modeling of the tidal bore on the Qiangtang River, China. J Hydraul Eng, 2007, 133: 130–138

16 Pan C H, Huang W R. Numerical modeling of suspended sediment transport affected by tidal bore in Qiantang Estuary. J Coast Res, 2010, 26: 1123–1132

17 Xie D F, Pan C H, Wu X G. Three-dimensional numerical modeling of tidal bore in the Qiantang Estuary based on FVCOM (in Chinese). Ocean Eng, 2011, 29: 47–52

18 Chen J Y, Luo Z D, Chen D C, et al. Formation of the river mouth bar and its historical evolution in the Qiantang Estuary (in Chinese). Acta Geogr Sin, 1964, 30: 109–123

19 Qian N, Xie H X, Zhou Z D, et al. The fluvial processes of the bid sand bar inside the Qiantang Estuary (in Chinese). Acta Geogr Sin, 1964, 30: 124–142

20 Li C X, Fan D D. Development of the Holocene Changjiang Delta and its influence on adjacent coastal sedimentary systems (in Chinese). J Palaeogeogr, 2009, 11: 115–122

21 Li B H, Wang Q, Li C X. Correlation of stratigraphic architecture of sub-deltas of the Changjiang River Delta (in Chinese). J Palaeogeogr, 2010, 12: 685–698

22 Martinius A W, Gowland S. Tide-influenced fluvial bedforms and tidal bore deposits (Late Jurassic Lourinhã Formation, Lusitanian Basin, Western Portugal). Sedimentology, 2011, 58: 285–324

23 Archer A W. Hierarchy of controls on cyclic rhythmite deposition: Carboniferous basins of eastern and mid-continental, U.S.A. In: Al-
exander C R, Davis R A Jr, Henry V J, eds. Tidalites: Processes and Products. Tulsa: SEPM, 1998. 59–68

24 Fan D D. Open-coast tidal flats. In: Davis R A Jr, Dalrymple R W, eds. Principles of Tidal Sedimentology. Heidelberg: Springer. 2011. 187–229

25 Zhang Z Z, Xu Z G. An approach to the sedimentation in the Qiantang Estuary (in Chinese). Mari Sci, 1987, (3): 10–15

26 Chen J Y, Liu C Z, Zhang C L, et al. Geomorphological development and sedimentation in Qiantang Estuary and Hangzhou Bay. J Coast Res, 1990, 6: 559–572

27 Sun H P, Li C X, Li P, et al. The tidal and sedimentary features of the lower reach of the Qiantang River (in Chinese). Shanghai Geol, 1990, (1): 62–71

28 Jiang G J, Zhang Z Z. Dynamical sedimentation in the Qiantang Estuary (in Chinese). J Hangzhou Univ (Nat Sci), 1995, 22: 306–312

29 Zhang G J, Li C X. The fills and stratigraphic sequences in the Qiantangjiang Incised Paleovalley, China. J Sediment Res, 1996, 66: 406–414

30 Lin C M, Li G Y, Zhuo H C, et al. Sedimentary facies of incised valley fillings of the late Quaternary in the Hangzhou Bay and shallow biogenic gas exploration (in Chinese). J Palaeogeogr, 2005, 7: 12–24

31 Li Y L. Characters of incised-valley filling sequences and the Late Quaternary environmental evolution in the Qiantang Estuary (in Chinese). Dissertation for the Doctoral Degree. Nanjing: Nanjing University, 2010

32 Chen L H. Effect of extensive regulation and reclamation engineers on the Qiantang bore height (in Chinese). Adv Water Sci, 2007, 18: 385–389

33 Xu H P, Zhang Y W, Xu C W, et al. Coastal seafloor observatory at Xiaoqushan in the East China Sea. Chin Sci Bull, 2011, 56: 2839–2845

34 Feng Y J, Li Y, Xie Q C, et al. Morphology and activity of sedimentary interfaces of the Hangzhou Bay (in Chinese). Acta Oceanol Sin, 1990, 12: 213–223

35 Xie D F, Wang Z B, Gao S, et al. Modeling the tidal channel morphodynamics in a macro-tidal embayment, Hangzhou Bay, China. Cont Shelf Res, 2009, 29: 1757–1767

36 Yu J, Cao Y. Long-term sediment erosion/deposition and deformation of river-bed in the Qiantang Estuary (in Chinese). J Mar Sci, 2006, 24: 28–38

37 Guo Y X, Fan D D, Zhao J. Grain-size characteristics and their applications to the intertidal subfacies division: A case study from Andong tidal flats in the Hangzhou Bay (in Chinese). Mar Geol Lett, 2004, 20: 9–14

38 Jia J J, Gao S, Xue Y C. Grain-size parameters derived from graphic and moment methods: A comparative study (in Chinese). Oceanol Limnol Sin, 2002, 33: 577–582

39 Passega R. Grain size representation by CM patterns as a geologic tool. J Sediment Res, 1964, 34: 830–847

40 Greb S F, Archer A W, Debore D G. Apogean-perigean signals encoded in tidal flats at the fluvio-estuarine transition of Glacier Creek, Turnagain Arm, Alaska: Implications for ancient tidal rhythmites. Sedimentology, 2011, 58: 1434–1452

41 Greb S F, Archer A W. Soft-sediment deformation produced by tides in a meizoseismic area, Turnagain Arm, Alaska. Geology, 2007, 35: 425–438

42 Posamentier H W, Walker R G. Deep-water turbidites and submarine fans. In: Posamentier H W, Walker R G, eds. Facies Models Revisited. Tulsa: SEPM, 2006. 397–520